Experimental Analysis of Motion Response, Mooring Loads, and Failure Redundancy of an Eight-Point System for the OCTABUOY Platform

Haitao Xu , Hong Zhou * , Xiao Xu

Posted Date: 15 May 2026

doi: 10.20944/preprints202605.1032.v1

Keywords: OCTABUOY platform; mooring design; hydrodynamic analysis; model tests

 doi:10.20944/preprints202605.1032.v1

Article

Experimental Analysis of Motion Response, Mooring Loads, and Failure Redundancy of an Eight-Point System for the OCTABUOY Platform

Haitao Xu, Hong Zhou * and Xiao Xu

School of Naval Architecture and Ocean Engineering, Jiangsu University of Science and Technology, Zhenjiang 212000, China

* Correspondence: zjcyzh@163.com

Abstract

To ensure the operational safety of the OCTABUOY platform used for offshore wind turbine installation in shallow waters, an eight-point symmetric mooring system was designed based on its octagonal structural configuration. The system provides high horizontal stiffness and balanced load distribution, enhancing stability under complex environmental conditions.Physical model tests were conducted under combined wind, wave, and current loading, considering multiple wave directions, environmental cases, and five draft conditions. The mooring tensions and six-degree-of-freedom motions were systematically analyzed to evaluate system performance and safety.Results show that the proposed mooring system effectively limits platform motions and maintains stable load-sharing characteristics. The minimum safety factor under the most unfavorable condition exceeds the design requirement. In addition, the system demonstrates good redundancy: after single-line failure, remaining mooring lines redistribute loads without progressive collapse. Draft and wave incident angle significantly influence peak tensions and motion responses, with smaller drafts and oblique wave directions producing relatively higher loads.The experimental results confirm the reliability and safety margin of the eight-point mooring system and provide practical guidance for the engineering application and operational assessment of the OCTABUOY platform in shallow-water wind installation projects.

Keywords: OCTABUOY platform; mooring design; hydrodynamic analysis; model tests

1. Introduction

With the rapid development of global offshore wind energy toward deeper waters and large-scale deployment, floating installation platforms have become essential equipment supporting offshore wind construction. Compared with conventional fixed installation vessels, floating structures offer greater adaptability to various sea areas, particularly in shallow-water transition zones and restricted regions [1–3]. The Octabuoy platform, an octagonal symmetric floating structure, has evolved from a conceptual design to practical engineering application in recent years. It is primarily used for the installation and maintenance of wind turbines in shallow-water environments with a design water depth of approximately 55 m. In such conditions, wave reflection effects are pronounced, and the coupled actions of wind, waves, and currents become more significant, imposing higher requirements on station-keeping accuracy and mooring safety margins [4–7].

The mooring system is the key structural component connecting the floating platform to the seabed and represents the only external restraint ensuring platform stability. Its performance directly determines the safety and operational reliability of the platform under extreme environmental conditions [8–10]. In recent years, extensive research has been conducted on the design and optimization of mooring systems for various floating structures, including multi-objective optimization approaches [11–13], multi-segment mooring analyses [14], the influence of mooring

 doi:10.20944/preprints202605.1032.v1

layout on structural responses, and the performance of taut mooring systems [15–17]. Meanwhile, three-dimensional potential flow theory has become a fundamental framework for hydrodynamic analysis of floating structures, playing a crucial role in predicting dynamic responses under combined wind–wave–current loading [18,19]. Scale-model experiments and wave incidence angle sensitivity analyses are widely employed to investigate motion characteristics under complex sea states, providing essential experimental evidence for engineering design [20–23].

In terms of mooring safety, the failure of individual mooring lines has attracted increasing attention. Previous studies have demonstrated that when one mooring line fails, the remaining lines must redistribute environmental loads, potentially leading to significantly increased tensions and even progressive failure [24–27]. Therefore, evaluating the redundancy capacity of multi-point mooring systems under extreme conditions and single-line failure scenarios is critical for ensuring long-term operational safety of floating platforms [28,29]. However, systematic experimental investigations of octagonal symmetric platforms operating in shallow-water wind installation scenarios remain limited [30], particularly under combined conditions involving multiple drafts, various incident angles, and single-line failure [31,32].

Moreover, the octagonal symmetric configuration of the Octabuoy platform differs significantly from conventional semi-submersible platforms, resulting in unique load transfer paths and restoring mechanisms [33–35]. Consequently, physical model tests are necessary to systematically examine mooring tension distributions, motion response characteristics, and safety margins under representative and extreme environmental combinations [36–39].

Based on the above considerations, this study conducts 1:60 scale physical basin experiments to evaluate the performance of an eight-point all-steel symmetric mooring system under various wave heights, periods, wind speeds, current velocities, incident angles, and draft conditions [40–43]. In addition, single-line failure scenarios are simulated under the most unfavorable environmental combinations to assess load redistribution capability and system redundancy. Through comprehensive comparison of full-condition matrices and abnormal conditions, the governing design case is identified, the influence of draft and wave direction on mooring performance is clarified, and the safety and reliability of the proposed eight-point mooring system for shallow-water wind installation applications are validated.

The findings of this study provide experimental evidence supporting the engineering application of the Octabuoy platform in shallow waters and offer valuable references for mooring design optimization and safety assessment of similar octagonal symmetric floating structures.

2. Research Object and Experimental Design

2.1. General Parameters of the Octabuoy Platform

This study focuses on the OCTABUOY wind turbine installation platform and its eight-point mooring system through physical model testing in a wave basin. The platform is primarily designed for wind turbine installation and maintenance operations in shallow-water regions, with a design water depth of approximately 55 m. Compared with deep-water floating structures, shallow-water environments are characterized by more pronounced wave reflection effects and stronger wind–wave–current interactions, which impose higher requirements on station-keeping stability and mooring safety margins.

The OCTABUOY platform adopts an octagonal floating body configuration with an approximately plane-symmetric geometry. The main dimensions are illustrated in Figure 1(a). The overall length and width are 94.944 m and 94.292 m, respectively, and the molded depth is 81.792 m. The height of the upper deck above the baseline is 60.95 m. The four main columns also function as ballast tanks, enabling adjustment of the draft by regulating ballast water, thereby accommodating different operational stages.

 doi:10.20944/preprints202605.1032.v1

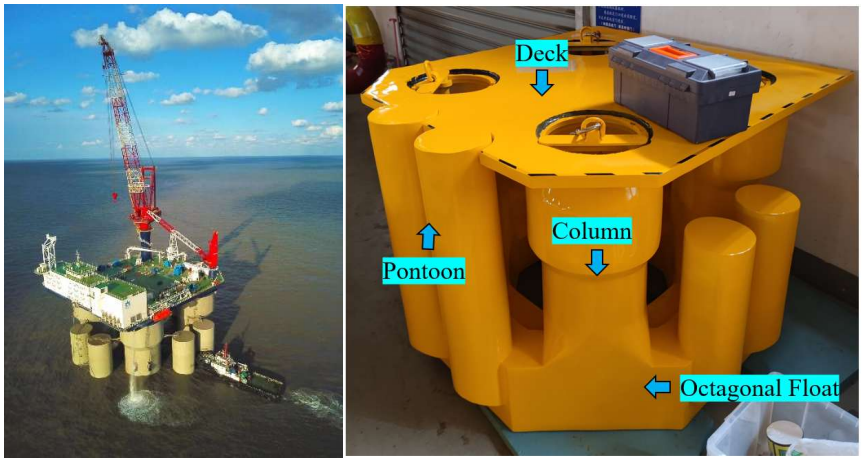

(**a**) Actual Ship (**b**) Octabuoy platform Main Structure Model

Figure 1. sketch map of Octabuoy platform.

The standard draft in the light condition is 9.5 m, while the maximum operational draft can reach 52 m. The displacement and moments of inertia vary significantly with draft, as shown in Table 1. As the draft increases, the inertial properties of the platform are enhanced, which influences both motion responses and mooring tension distributions. Therefore, multiple draft conditions were considered in the experimental design to comprehensively evaluate system performance under different mass and inertia characteristics.

Table 1. Platform parameters under different draft operating conditions.

Items	**operational condition**				
Draft (m)	9.5	20	30	40	50
VCG(m) (above the baseline)	32.26	20.88	19.9	20.11	21.37
Displacement(t)	40600	74747	100275	124039	143338
roll moment of inertia(kg·m2)	5.12×107	8.69×107	1.06×108	1.25×108	1.38×108
pitch moment of inertia(kg·m2)	5.5×107	9.08×107	1.1×108	1.29×108	1.42×108
yaw moment of inertia(kg·m2)	5.32×107	1.01×108	1.34×108	1.65×108	1.84×108

2.1. Similarity Criteria and Experimental Conditions

Physical model testing was adopted to investigate the motion responses and mooring tension characteristics of the platform under various environmental loads. The experiments were conducted in a comprehensive wave basin equipped with wave generation, current simulation, and wind field generation capabilities.

Considering experimental constraints and facility limitations, a geometric scale ratio of 1:60 was selected. The model was designed according to geometric similarity and Froude similarity principles to ensure dynamic similarity for gravity-dominated free-surface flow. The scaling relationships for the relevant physical quantities are summarized in Table 2.

Table 2. Summary of physical quantity scales used in the experiment.

Item	**Symbol**	**Scale factor**	**Item**	**Symbol**	**Scale factor**
Linear scale	L_s / L_m	λ	Period	T_s / T_m	$\lambda^{1/2}$
Area	A_s / A_m	λ^2	Frequency	f_s / f_m	$\lambda^{-1/2}$
Volume	∇_s / ∇_m	λ^3	Density of water	ρ_s / ρ_m	γ
Linear velocity	V_s / V_m	$\lambda^{1/2}$	Mass (displacement)	Δ_s / Δ_m	$\gamma\lambda^3$

 doi:10.20944/preprints202605.1032.v1

Linear acceleration	a_s / a_m	1	Force	F_s / F_m	$\gamma\lambda^3$
Angle	ϕ_s / ϕ_m	1	Moment / Torque	M_s / M_m	$\gamma\lambda^4$
Angular velocity	φ_s / φ_m	$\lambda^{-1/2}$	Moment of inertia	I_s / I_m	$\gamma\lambda^5$

Both the main platform structure and the mooring system were manufactured according to the selected scale ratio, as illustrated in Figure 1(b). Detailed model parameters are provided in Table 3. The systematic scaling design ensures that the experimental results can be reasonably extrapolated to prototype conditions.

Table 3. Platform parameters under different draft operating conditions.

Items	**operational condition**				
Draft (m)	0.158	0.333	0.5	0.667	0.833
VCG(m) (above the baseline)	0.538	0.348	0.332	0.335	0.356
Displacement(t)	183.8735	346.6441	452.9133	560.2484	647.4164
roll moment of inertia(kg·m2)	64.21243	109.0736	132.9731	156.8016	172.6443
pitch moment of inertia(kg·m2)	69.01764	113.9163	137.8821	161.9308	178.3618
yaw moment of inertia(kg·m2)	66.76182	126.3349	168.5072	206.5974	231.1047

2.3. Coordinate System and Environmental Direction Definition

To ensure consistency in data analysis, a global right-handed coordinate system was established, as shown in Figure 2. The origin is located at the center of gravity of the platform under the corresponding draft condition. The X-axis points toward the bow, the Y-axis toward the port side, and the Z-axis vertically upward. Environmental load directions are defined relative to the platform heading. Loads acting along the positive X-axis are defined as 0°, while those acting along the positive Y-axis are defined as 90°. This definition provides a unified framework for analyzing platform motion responses and mooring tensions under different incident angles. The coordinate system remains unchanged throughout the experiments and subsequent data processing to ensure comparability of motion and load analyses.

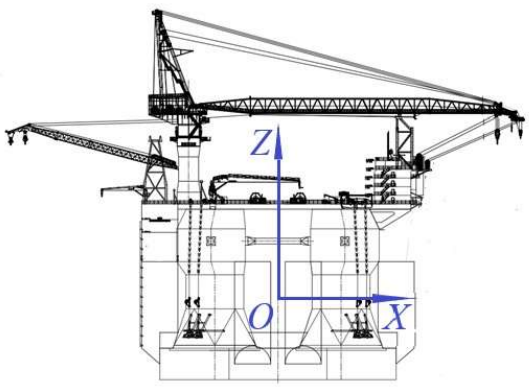

(**a**) side view

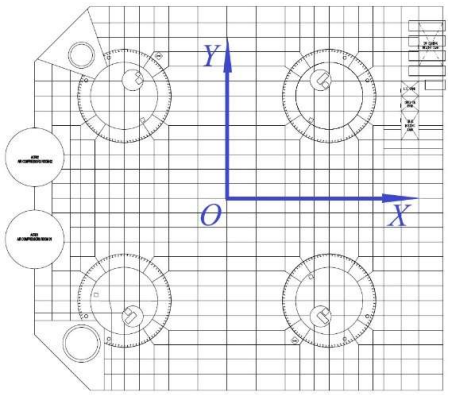

(**b**) top view

 doi:10.20944/preprints202605.1032.v1

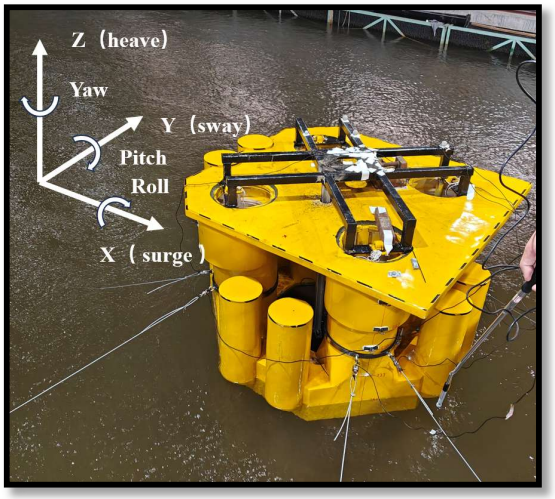

(**c**) model test

Figure 2. Coordinate systems.

2.4. Eight-Point Mooring System Design

Based on the octagonal symmetric geometry of the OCTABUOY platform, an eight-point centrally symmetric mooring system was developed, as shown in Figure 3. The mooring points are arranged on the four main columns, with eight mooring lines uniformly distributed in the horizontal plane. The angle between adjacent mooring lines is 45°.

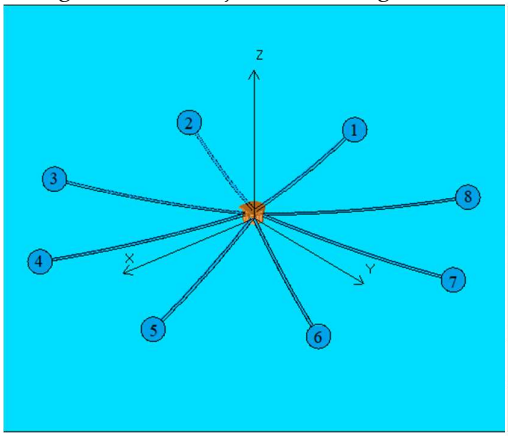

(**a**) Model of mooring system with 8 lines

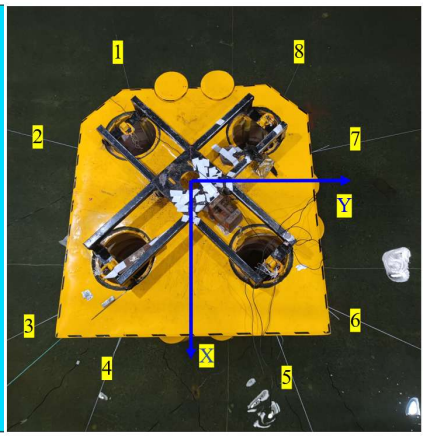

(**b**) model test

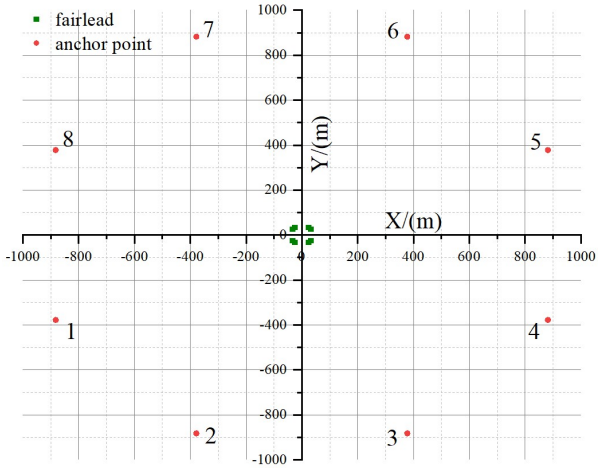

(**c**) coordinate diagram of morring point

 doi:10.20944/preprints202605.1032.v1

Figure 3. Arrangement of mooring system.

The system adopts an all-steel-wire configuration without chain segments. The prototype mooring line length is 920 m, with a horizontal mooring radius of 882 m. The main parameters of the mooring lines, including diameter, submerged weight per unit length, axial stiffness (EA), and breaking load, are listed in Table 4.

Table 4. The detailed mechanical properties of mooring line.

Actual Ship	**Length (m)**	**Diameter (mm)**	**Wet weight (kg/m)**	**Stiffness EA(N)**	**Breaking load(kN)**
	920	90	33.9	4.9e8	5100
Model	**Length (m)**	**Diameter (mm)**	**Wet weight (g/m)**	**Stiffness EA(N)**	**Breaking load(N)**
	15.33	1.5	9.42	2.27e4	23.6

The symmetric layout is consistent with the platform geometry and enables balanced restoring force distribution under multi-directional environmental loading. Compared with conventional low-point mooring systems, the eight-point configuration provides a more refined load-sharing mechanism, reducing peak tension in individual lines and enhancing redundancy under extreme conditions.

In addition, potential single-line failure scenarios were considered in the experimental program. The tension variations in the remaining mooring lines were analyzed to evaluate system stability and safety margins under abnormal conditions.

2.5. Marine Environmental Loading Conditions

To simulate realistic offshore operational conditions, combined wind, wave, and current loads were applied. Irregular waves were generated using the JONSWAP spectrum with a peak enhancement factor $\gamma = 2$, representing typical developing sea states.

Two representative environmental cases were defined (Table 5). For each case, wave incident angles ranging from 0° to 90° (at 22.5° intervals) and five draft conditions were considered, forming a comprehensive test matrix. This systematic arrangement enables the investigation of motion response characteristics, mooring tension distributions, and safety margins under various environmental directions and platform mass states, thereby providing experimental evidence for the engineering applicability of the eight-point mooring system..

Table 5. Marine Design Environmental Loads for the Octabuoy Wind Turbine Installation Platform.

Items	**Significant wave height Hs (m)**	**Peak spectral period Tp (s)**	**Current velocity(m/s)**	**Wind velocity(m/s)**	**Wave/Current/Wind direction(◦)**	**Draft（m）**
Case1	1.5	7.5	1.0	13.8	0-90，interval of 22.5	9.5/20/30/40/50
Case2	2	8.5	1.5	17.1	0-90，interval of 22.5	9.5/20/30/40/50

3. Model Experiment

3.1. Measurement Equipment and Experimental Facility

To evaluate the performance of the proposed eight-point mooring system for the OCTABUOY platform, physical model experiments were conducted in the wave basin of the State Key Laboratory at Jiangsu University of Science and Technology.

The wave basin has a maximum operating water depth of 1 m. The wave height range is 0.05–0.25 m, and the wave period range is 0.5–2.5 s. The facility is capable of generating regular waves,

 doi:10.20944/preprints202605.1032.v1

superimposed waves, and various irregular wave spectra. It is also equipped with a current-generation system and a movable wind simulator, enabling combined wind–wave–current loading conditions, as illustrated in Figure 4.

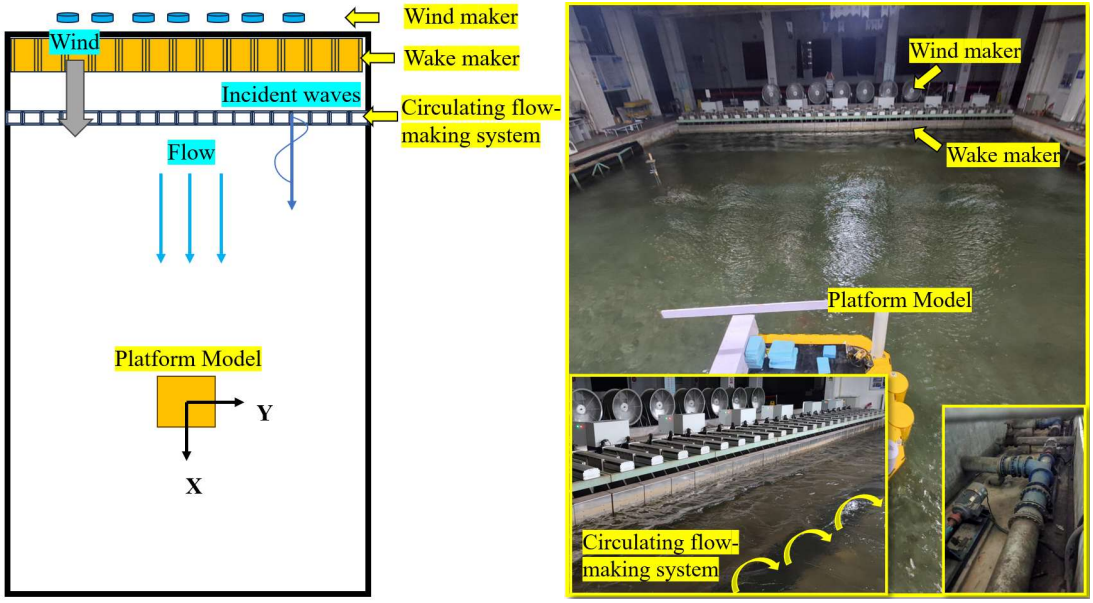

(**a**) top view (**b**) Test wave basin

Figure 4. General arrangement of the Irregular wave model test.

The model scale ratio was selected as 1:60. Both the main platform structure and the mooring system were fabricated according to the same geometric scaling. The principal parameters of the prototype and the model are summarized in Table 6.

Table 6. Principal particulars of module platform and the mooring system.

Items	Parameter	Prototype	Model
Single model	Length(m)	94.944	1.582
	Width(m)	94.292	1.572
	Moulded depth(m)	81.792	1.363
column	Number of columns	4	4
	Diameter(m)	20	0.333
	Height(m)	42.761	0.713
pontoon	Number of pontoons	8	8
	Diameter(m)	12.5	0.208
	Height of short pontoons (m)	35.46	0.591
	Height of high pontoons (m)	55.45	0.924
transverse brace	Length(m)	22.567	0.376
	Diameter(m)	2	0.033
Octagonal floating body	Height(m)	16.38	0.273
	side length(m)	33.88	0.565

To achieve high-precision motion measurement, an optical motion tracking system was installed on the side of the basin, as shown in Figure 5. The system consists of multiple high-resolution cameras that detect reflective markers mounted on the platform, enabling real-time measurement of six-degree-of-freedom (6-DOF) motions. The system was carefully calibrated before testing to ensure spatial accuracy met the experimental requirements. To record environmental loading data, a wave probe was installed in front of the platform to measure incident wave elevations in real time. In addition, high-precision tension sensors were installed on all eight mooring lines to synchronously collect mooring tension data. All sensors were calibrated prior to testing to ensure data reliability.

 doi:10.20944/preprints202605.1032.v1

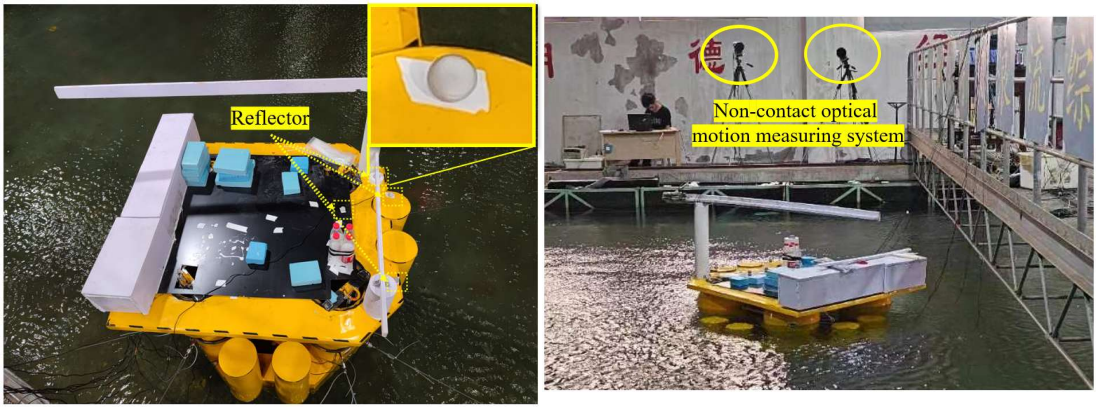

Figure 5. The multidimensional monitoring system of FOWT in wave basin test.

3.2. Overall Experimental Configuration

Based on the prototype design water depth of 55 m, the corresponding model water depth was 0.917 m under the 1:60 scale ratio. The overall experimental arrangement is shown in Figure 6, including the platform model, mooring system, wind–wave–current loading devices, and tension measurement system.

(**a**) typical photographs of the model test (**b**) Model of Tension sensor

Figure 6. Photograph of the model test.

All test cases were conducted under irregular wave conditions combined with prescribed wind and current velocities to simulate realistic offshore operating environments. For each test condition, platform motions and mooring line tensions were simultaneously recorded. Through systematic combination of environmental parameters, the load distribution characteristics under different incident directions and draft conditions were analyzed.

3.3. Verification of Mooring System Stiffness

To evaluate the overall stiffness performance of the eight-point mooring system, a quasi-static restoring force test was conducted under the smallest draft condition (0.158 m in model scale, corresponding to 9.5 m in prototype). At this draft, all mooring lines were fully tensioned.The test procedure was as follows: horizontal external forces were gradually applied in both the X and Y directions, causing the platform to slowly shift to new equilibrium positions. At each load level, measurements were recorded after system vibrations decayed and steady-state conditions were reached. The load was then incrementally increased to the maximum value and subsequently reduced following the same procedure, thereby obtaining complete loading–unloading restoring curves.To avoid exceeding the mooring line breaking load (5100 kN in prototype scale), the maximum applied model load was determined as 65 N according to the similarity law. This value corresponds

 doi:10.20944/preprints202605.1032.v1

to the prototype safety limit condition. The maximum load was divided into five incremental stages (13 N, 26 N, 39 N, 52 N, and 65 N) to ensure quasi-static loading and minimize dynamic effects on the restoring response.

The displacement responses in the X and Y directions are shown in Figure 7. Due to minor fluctuations during testing, time-averaged values were calculated for each load stage to obtain smoother restoring curves, as illustrated in Figure 8.The results indicate that under the maximum applied load, the maximum horizontal displacement of the model was approximately 40 mm, corresponding to 2.4 m at prototype scale. After load release, the platform nearly returned to its initial position, with a residual displacement of approximately 2.5 mm (about 0.15 m in prototype scale). This residual displacement is within acceptable engineering limits, indicating that the mooring system exhibits satisfactory restoring capability and structural stiffness.The restoring curves demonstrate an approximately linear relationship within the tested load range, suggesting that the mooring system operated within the elastic regime without noticeable nonlinear instability behavior.

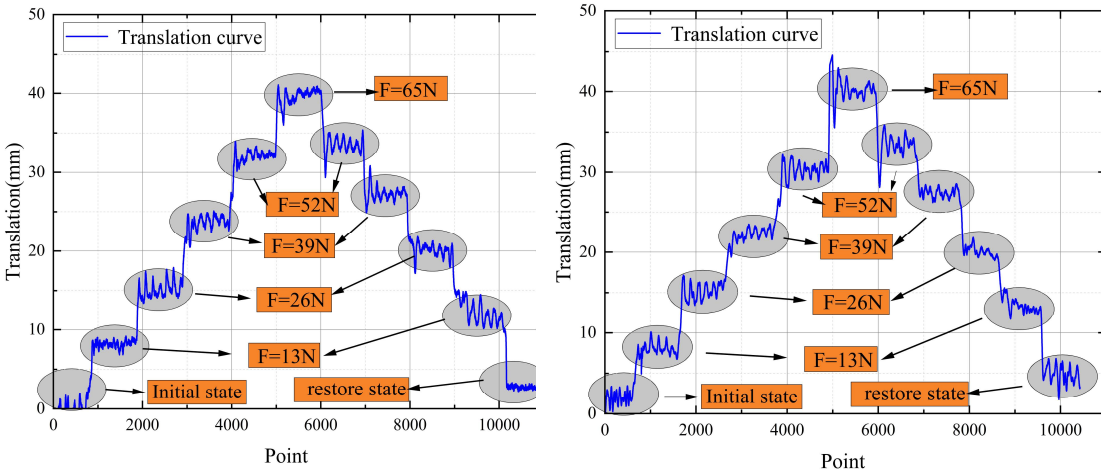

(**a**) X direction (**b**) Y direction

Figure 7. Translation Curve.

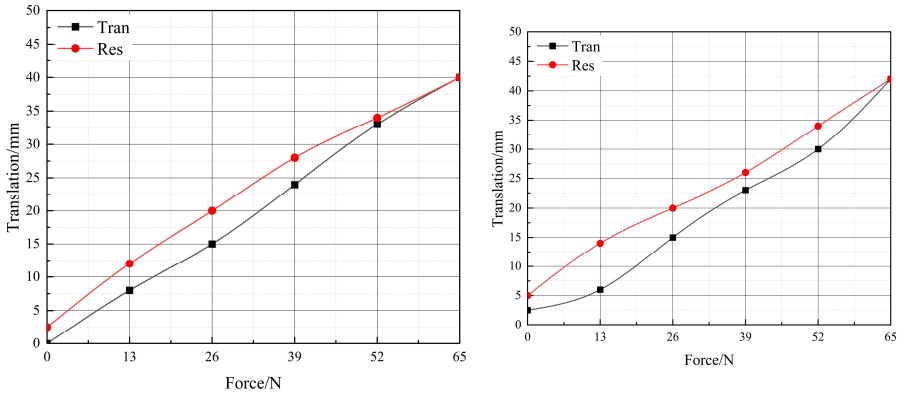

(**a**) Applying a force in the x-direction. (**b**) Applying a force in the y-direction.

Figure 8. Restoring Force Curve.

4. Discussion

Based on the results of the wave basin experiments, the mooring tension characteristics and platform motion responses under different environmental conditions, incident wave angles, and draft configurations are systematically analyzed in this chapter. Particular attention is given to the load-sharing behavior of the eight-point mooring system, the governing conditions under extreme

 doi:10.20944/preprints202605.1032.v1

scenarios, the influence of draft on safety margins, and the redundancy performance under single-line failure. All results are presented in prototype scale.

4.1. Mooring Tension Characteristics

4.1.1. Tension Distribution Pattern and Directional Characteristics

Among the numerous operating conditions analyzed for the Octabuoy platform, a representative case was selected for detailed comparison. Figure 9 presents the time histories of the eight mooring line tensions obtained from both the physical model test and numerical simulation under a draft of 9.5 m and a 0° incident angle (Case 1).In the wave basin experiment, each irregular wave condition was tested for approximately 20 minutes. Given the relatively high sampling frequency, each case contains nearly 80,000 data points. Under such a large dataset, direct interpretation of the full time series becomes challenging. Therefore, for clearer comparison, the maximum tension and time-averaged tension of each mooring line were extracted and summarized, as shown in Figure 10.The results are presented in a polar coordinate system. The angular position corresponds to the environmental load direction (wind, wave, and current), which is defined consistently with the global coordinate system. This representation allows intuitive visualization of the relative orientation between environmental loading and mooring line arrangement, as well as the spatial distribution of tension magnitudes. The numerical labels in the figure correspond to the mooring line numbering defined in the system layout.

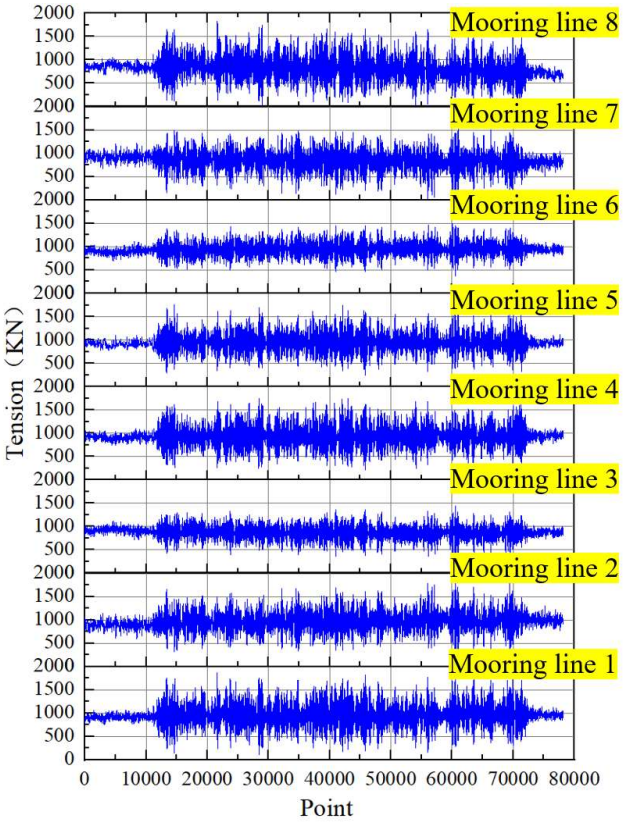

Figure 9. Mooring line tension curve.

 doi:10.20944/preprints202605.1032.v1

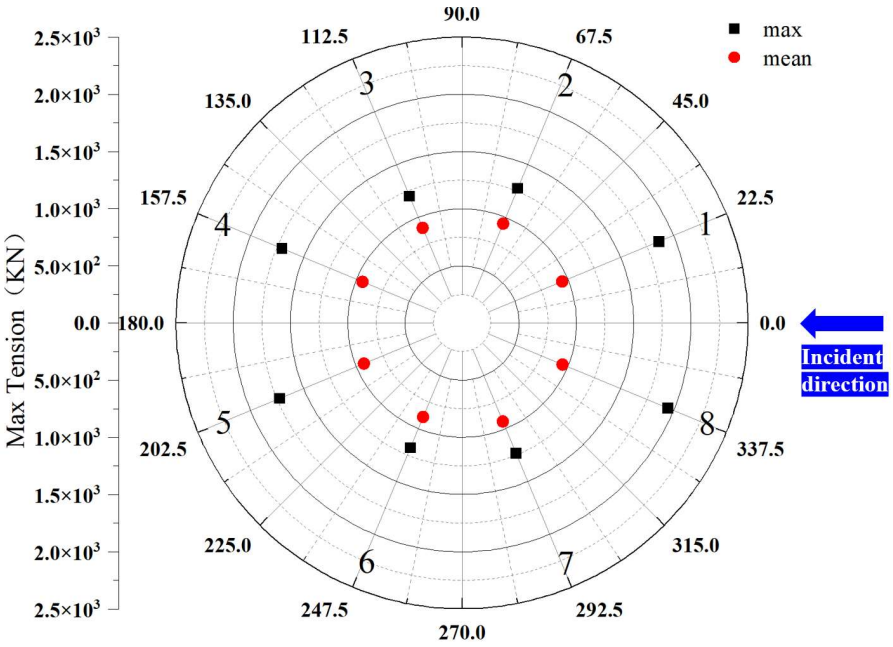

Figure 10. Mooring line tension comparison.

From the comparative results, several key physical characteristics can be observed.

(1) Directional Load Sharing Mechanism

It is evident that the majority of the external environmental loads acting on the Octabuoy platform are primarily resisted by the windward and leeward mooring lines. Specifically, Lines 1 and 8 experience the highest maximum tensions, followed by Lines 4 and 5. The mooring tensions on the windward side are generally larger than those on the leeward side.This distribution is directly related to the geometric alignment between the mooring lines and the environmental loading direction. The lines whose orientations are closer to the direction of wind, wave, and current receive larger force projections. In contrast, lines approximately orthogonal to the loading direction carry significantly smaller horizontal components.

From a structural mechanics perspective, the octagonal symmetric configuration ensures that the restoring forces are distributed in a balanced manner around the platform center. When subjected to unidirectional loading (0° case), the platform undergoes predominantly surge-dominated oscillatory motion. Because all eight mooring lines remain in tension, the system behaves as a fully restrained restoring network. The symmetric layout prevents excessive force concentration on a single line and promotes distributed load sharing.The observation that both windward and leeward lines exhibit relatively high tensions further indicates that the platform does not experience purely translational drift. Instead, it performs periodic forward–backward oscillatory motion under irregular wave excitation. During forward motion, windward lines are primarily stretched; during backward motion, the opposite lines become dominant. This alternating tension mechanism is characteristic of fully pre-tensioned multi-point mooring systems.Therefore, the eight-point symmetric arrangement effectively transforms environmental excitation into distributed restoring forces, enhancing overall system stability.

(2) Relationship Between Maximum and Mean Tension

A comparison between maximum and mean tensions reveals that the average tension of each mooring line is close to 950KN, a value slightly higher than the pre-tension of 900KN. This result is physically consistent with the oscillatory nature of the platform response under irregular wave conditions. The near-950KN mean tension indicates that the platform does not experience sustained directional drift under the tested conditions. Instead, the mooring system primarily provides dynamic restoring resistance to periodic motion. The symmetry of the system ensures that tension

 doi:10.20944/preprints202605.1032.v1

fluctuations occur around an equilibrium state without long-term bias in any specific direction.This characteristic confirms that the Octabuoy platform operates in a dynamically balanced state under the combined wind–wave–current environment.From a safety evaluation perspective, the structural integrity of mooring systems is governed by extreme loads rather than mean values. Therefore, subsequent analyses focus on maximum tension values to assess design safety margins. The maximum tension represents the critical loading condition for strength verification, while the mean value mainly reflects dynamic equilibrium behavior.

The tension distribution pattern can be interpreted through the coupled interaction between platform motion and mooring elasticity. Under environmental excitation, the platform displacement induces elongation of specific mooring lines. Due to the axial stiffness of the steel wire ropes, restoring forces are generated proportional to line deformation.The eight-line symmetric configuration increases the global restoring stiffness in both surge and sway directions. As a result, motion amplitudes are constrained, and load redistribution occurs naturally among adjacent lines. This distributed stiffness mechanism explains why peak tensions are concentrated in lines aligned with the loading direction, while the remaining lines still participate in load sharing.Overall, the experimental results confirm that the eight-point symmetric mooring system provides effective directional load resistance, balanced force distribution, and stable oscillatory behavior under irregular wave loading.

4.1.2. Influence of Draft on Maximum Tension

The variation of maximum mooring tensions under different draft conditions is presented in Figure 11. It can be clearly observed that, for all mooring lines, the peak tensions decrease progressively as draft increases. This trend remains consistent under different environmental incidence angles, indicating a robust sensitivity relationship between draft and mooring load levels.Under the 0° incident condition, the largest tensions consistently occur in Lines 1 and 8, followed by Lines 4 and 5, which is consistent with the directional load-sharing characteristics discussed in Section 4.1.1. This confirms that the spatial alignment between mooring lines and environmental loading direction governs the peak tension distribution regardless of draft variation.Taking Line 1 as an example, when the draft increases from 9.5 m to 50 m, the maximum tension decreases from 1890 kN to 1158 kN, corresponding to an approximately 40% reduction. Such a substantial decrease demonstrates that draft is a dominant parameter affecting mooring safety margins.

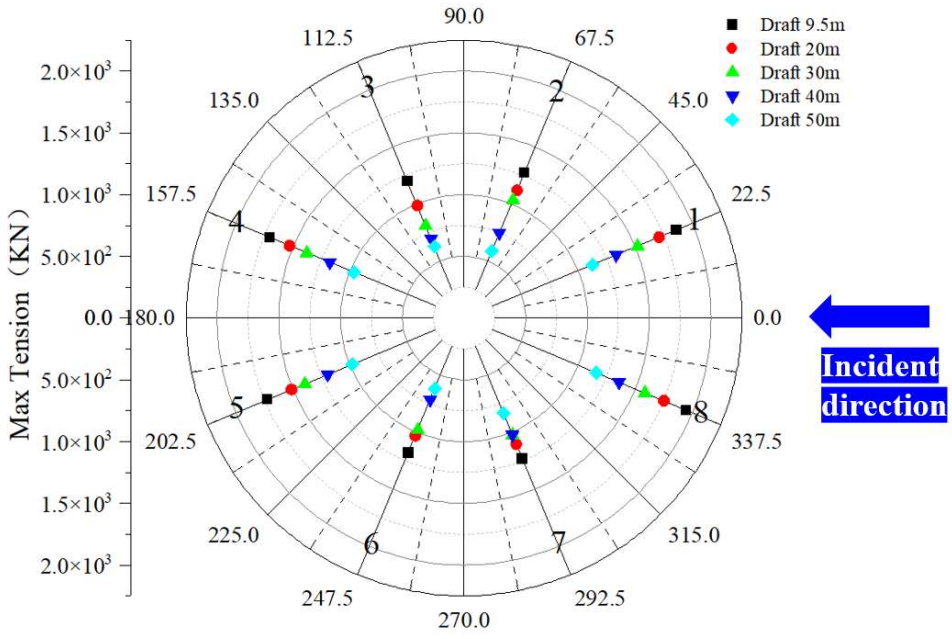

 doi:10.20944/preprints202605.1032.v1

Figure 11. Mooring Tension of Case1 at 0° Incidence Angle under Different Drafts.

The observed trend can be explained from multiple coupled physical perspectives.

(1) Geometric Catenary Effect and Line Configuration

As draft increases, the vertical position of the fairlead and the submerged length of the mooring lines change accordingly. A deeper draft modifies the overall geometric configuration of the mooring system, resulting in a more relaxed catenary shape under horizontal loading. In shallow draft conditions, mooring lines tend to exhibit larger horizontal components of tension due to increased geometric stiffness and reduced vertical compliance. As draft increases, the effective horizontal stiffness of the mooring system decreases, allowing greater redistribution of deformation into vertical components. Consequently, the peak horizontal tension under extreme environmental loading is reduced.This geometric nonlinearity plays a critical role in determining the load–displacement response of multi-point mooring systems.

(2) Enhancement of Hydrostatic Stability

Increasing draft significantly lowers the center of gravity of the Octabuoy platform relative to the waterline. This results in improved initial stability and increased righting moment under environmental loading.From a stability perspective, a deeper draft increases the metacentric-related restoring characteristics and enhances the platform's resistance to overturning induced by wind and wave forces. As a result, the required restoring force from the mooring system decreases, leading to lower peak tensions.Therefore, part of the tension reduction is directly associated with improved hydrostatic stability.

(3) Hydrodynamic Damping and Added Mass Effects

With increasing draft, the submerged volume of the platform increases. This leads to enhanced hydrodynamic damping and added mass effects.Higher added mass increases the inertia of the system, which reduces motion amplitudes under wave excitation. Simultaneously, increased radiation damping dissipates more wave energy. Both effects contribute to suppressing surge and pitch responses.Since mooring tension is strongly correlated with platform motion amplitude, reduced motion directly leads to reduced peak tension.This demonstrates that mooring loads are not only determined by environmental force magnitude but are also governed by the dynamic response characteristics of the coupled system.

(4) Reduction of Wind Load Exposure

As draft increases, a larger portion of the platform structure becomes submerged. Consequently, the effective wind-exposed area above the waterline decreases.In addition, the mooring lines themselves gradually descend deeper below the free surface. This reduces the direct wind-induced horizontal loading on both the platform and the exposed segments of the mooring lines.Therefore, the overall environmental loading transferred to the mooring system decreases with increasing draft.

Within the range investigated in this study, the 9.5 m draft condition consistently produces the highest mooring tensions under all incident angles. This indicates that the shallowest draft corresponds to the most unfavorable structural loading state.Therefore, the 9.5 m draft is identified as the controlling design condition for the Octabuoy mooring system.This conclusion is of significant engineering importance, as it defines the critical operational scenario that should be prioritized in structural verification and safety assessment. Based on the identification of the 9.5 m draft as the governing condition, the subsequent section focuses on analyzing mooring tension characteristics under multiple wave incidence angles to further evaluate directional sensitivity and design robustness.

4.1.3. Extreme Incident Angles and Governing Design Condition

For the critical draft of 9.5 m, the maximum mooring tensions under different wave incidence angles are further investigated, as illustrated in Figure 12. Two representative sea states (Case 1 and Case 2) are compared to evaluate the sensitivity of the mooring system to environmental severity. Overall, Case 2, characterized by larger significant wave height and longer spectral peak period,

 doi:10.20944/preprints202605.1032.v1

consistently generates higher peak mooring tensions than Case 1. This indicates that the extreme response of the system is strongly influenced by the energy level and frequency characteristics of the irregular wave spectrum.

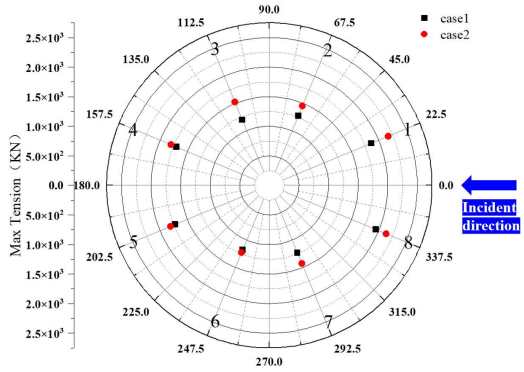

(**a**) 0 incident angle

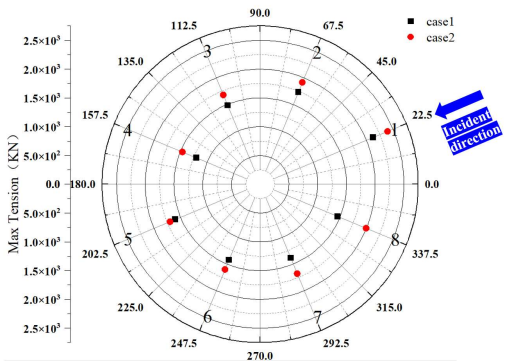

(**b**) 22.5 incident angle

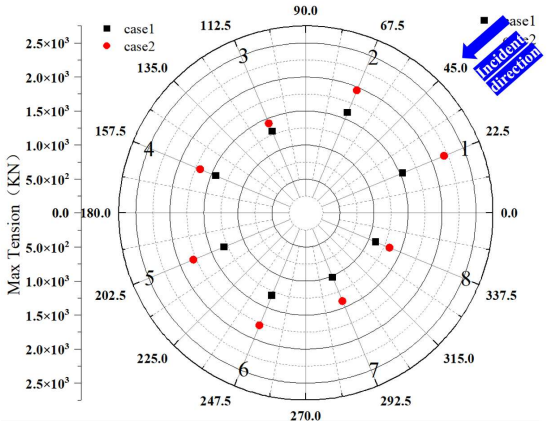

(**c**) 45 incident angle

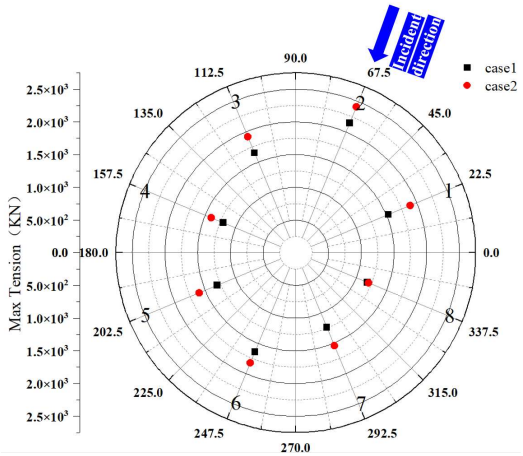

(**d**) 67.5 incident angle

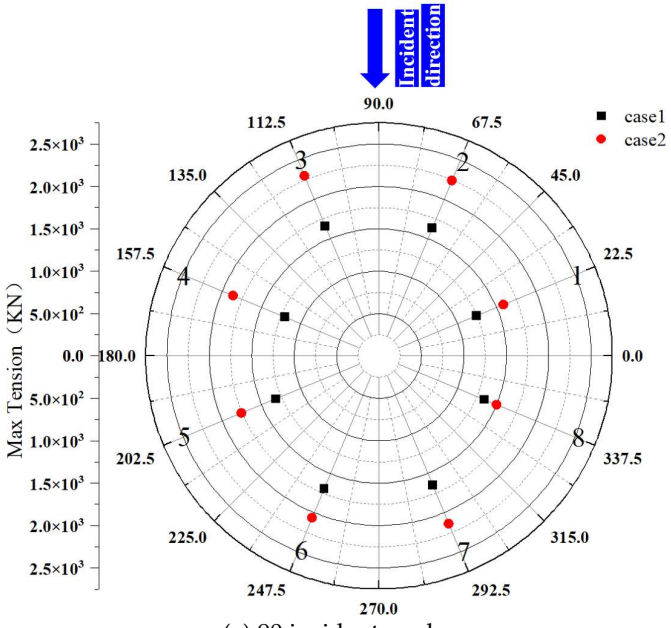

(**e**) 90 incident angle

Figure 12. Maximum Mooring Tension Calculation Results.

Although the tension distribution varies with wave direction, all computed maximum values remain below the design breaking load of 5100 kN, demonstrating that the mooring system maintains

 doi:10.20944/preprints202605.1032.v1

adequate structural safety under the considered extreme conditions.A clear directional dependency is observed in the results. The highest mooring tensions occur at 22.5° and 67.5° wave incidence angles rather than at 0° or 90° cases. This phenomenon can be explained from a force decomposition and symmetry perspective.

The eight-point mooring configuration is uniformly distributed with 45° spacing, forming a geometrically symmetric restraint system. When environmental loading acts along 0° (principal axis), the external forces are primarily aligned with one symmetric direction, allowing relatively balanced load sharing between opposite mooring lines. However, when the wave direction deviates from the principal axes—particularly at 22.5° and 67.5°—the environmental load projection becomes unevenly distributed among adjacent mooring lines. In these oblique loading conditions, one mooring line approaches alignment with the resultant environmental force vector, leading to a maximum directional load component along that line. Meanwhile, the adjacent lines provide incomplete symmetric compensation, resulting in localized tension amplification.From a structural mechanics viewpoint, this behavior reflects the directional stiffness variation of the symmetric mooring system. Although the platform configuration is geometrically symmetric, the equivalent horizontal restoring stiffness is not isotropic. Under oblique excitation, the vector summation of mooring restoring forces requires larger differential tensions among lines to satisfy equilibrium conditions. Consequently, peak line tension increases even when the overall environmental load magnitude remains unchanged.

Furthermore, the coupled motion response of the platform contributes to the observed tension pattern. Previous motion analyses indicate that oblique wave incidence enhances the coupling between surge, sway, and yaw motions. This multi-degree-of-freedom interaction increases the horizontal displacement amplitude and rotational response, which directly influences mooring line elongation. Since mooring tension is governed by both geometric nonlinearity and axial stiffness, even moderate increases in platform displacement can significantly amplify line loads in extreme sea states.

The results therefore confirm that the maximum mooring tension is not solely determined by wave height, but by the combined effects of wave direction, structural symmetry, and motion–restoring force coupling. Among all tested combinations, the 22.5° wave incidence under Case 2 conditions produces the highest peak tension and thus represents the governing design condition for the present mooring system at 9.5 m draft. This identification of the critical loading scenario provides a rational basis for structural strength verification and ensures that subsequent safety and redundancy assessments are conducted under the most unfavorable yet physically justified environmental configuration.

4.1.4. Wave Spectrum Characteristics and Response Mechanism

In the present study, irregular wave conditions were generated based on the JONSWAP spectrum with a peak enhancement factor $\gamma = 2$, representing a typical developing sea state. Compared with regular waves, the JONSWAP spectrum concentrates wave energy within a narrow frequency band around the spectral peak, while the energy content outside this dominant region decreases rapidly. Therefore, the dynamic response of the floating platform and the associated mooring tension is primarily governed by the spectral peak frequency and its surrounding bandwidth.

For large floating structures such as the Octabuoy platform, the natural periods in surge, sway, and low-frequency drift motions are generally much longer than the dominant wave periods. As a result, the mooring system response is mainly influenced by low-frequency components induced by second-order wave effects rather than by high-frequency wave oscillations. The high-frequency wave components predominantly affect local wave loading but contribute less to the peak mooring tension due to the substantial mass, inertia, and hydrodynamic damping of the platform.

Under irregular wave excitation, the platform exhibits stochastic oscillatory behavior around its equilibrium position rather than sustained drift. The maximum mooring tensions observed in the

 doi:10.20944/preprints202605.1032.v1

experiments correspond to combined effects of wave-induced low-frequency motions and environmental load projections along specific mooring directions. This explains why the peak tensions occur under oblique wave incidence angles, where the projected environmental load components along certain mooring lines are maximized.

Moreover, the Case 2 sea state produces larger mooring tensions and motion amplitudes compared with Case 1, which can be attributed to the increased significant wave height and the higher spectral energy level. The greater energy input within the dominant frequency band enhances the excitation of surge-dominated motions, thereby increasing the dynamic tension response of the mooring system. However, no abnormal amplification phenomenon was observed, indicating that the spectral peak frequency does not coincide with the dominant natural frequency of the coupled platform–mooring system.

Overall, the experimental results demonstrate that the mooring tension behavior of the Octabuoy platform under irregular wave conditions is primarily controlled by low-frequency dynamic responses governed by the energy distribution of the JONSWAP spectrum. This confirms that the identified critical environmental combinations are physically consistent with the wave energy characteristics and the dynamic properties of the platform–mooring coupled system.

4.2. Rigid Body Motion Response

The rigid-body motion responses of the Octabuoy platform were evaluated under different draft conditions and wave incidence angles using the measured maximum values extracted from irregular wave tests. The six-degree-of-freedom motion responses are summarized in Tables 7 and 8.The objective of this section is to clarify the influence of environmental directionality and draft variation on global motion behavior, and to examine the coupling relationship between platform motion and mooring system performance.

Table 7. The motion response of Case 1 at a 0° incidence angle.

Case	Degree of freedom	Draft (m)				
		9.5	20	30	40	50
1	x（m）	1.534	1.322	1.099	0.988	0.718
	y（m）	0.32	0.33	0.29	0.31	0.25
	rx（°）	0.295	0.245	0.211	0.189	0.156
	ry（°）	3.482	3.126	2.734	2.415	1.796

Table 8. Motion responses for all scenarios at a draft of 9.5 meters.

Case	Degree of freedom	incident angle				
		0°	22.5°	45°	67.5°	90°
1	x（m）	1.534	1.345	1.109	0.869	0.37
	y（m）	0.32	0.923	1.116	1.356	1.561
	rx（°）	0.295	2.369	3.224	3.864	3.543
	ry（°）	3.482	3.563	2.945	1.987	0.236
2	x（m）	1.621	1.463	1.221	1.082	0.45
	y（m）	0.51	1.101	1.278	1.463	1.654
	rx（°）	0.425	2.867	3.336	3.998	3.645
	ry（°）	3.862	3.681	3.002	3.121	0.333

Overall, the results demonstrate that the motion characteristics of the platform are strongly governed by both hydrostatic stability and environmental loading direction. Under the 0° wave incidence condition, the influence of draft variation is particularly evident. As the draft increases from 9.5 m to 50 m, the maximum surge displacement decreases from 1.534 m to 0.718 m, and the maximum pitch angle decreases from 3.482° to 1.796°. Similar reduction trends are observed for the other degrees of freedom.

 doi:10.20944/preprints202605.1032.v1

(1) This systematic decrease in motion amplitude with increasing draft can be interpreted from a stability and hydrodynamic perspective. First, increasing draft lowers the center of gravity relative to the waterline, thereby enhancing hydrostatic righting moments and improving initial stability. A deeper draft increases the metacentric restoring effect, reducing the tendency of the platform to experience large rotational excursions under environmental loading. Second, the submerged volume increases, which enhances hydrodynamic added mass and radiation damping effects. These mechanisms reduce the dynamic amplification of motion responses under irregular wave excitation. Third, the change in draft modifies the mooring geometry, resulting in more favorable tension angles and improved horizontal restoring efficiency. The combined effect of these mechanisms leads to reduced rigid-body motion amplitudes at larger drafts.

(2) The directional characteristics of the motion responses are further revealed by the results at different wave incidence angles for the critical draft of 9.5 m. The maximum surge displacement occurs under 0° incidence, while the maximum sway displacement occurs under 90° incidence, which is consistent with the definition of the global coordinate system. This indicates that the principal motion components are aligned with the dominant environmental excitation direction.

(3) when evaluating the total horizontal response through vector combination of surge and sway components, it is observed that the largest resultant planar displacement occurs under oblique wave incidence conditions, particularly at 22.5° and 67.5°. In these cases, both surge and sway motions are simultaneously activated due to the non-alignment between the environmental load vector and the principal axes of symmetry. The superposition of the two horizontal components leads to an increased overall displacement magnitude, even though neither component individually reaches its maximum value. Under the most unfavorable sea state, the maximum resultant horizontal displacement reaches approximately 3.6 m at prototype scale.This behavior highlights the importance of oblique loading scenarios in assessing global system performance. For symmetric platforms such as Octabuoy, oblique environmental excitation represents a condition in which the equivalent restoring stiffness in the horizontal plane becomes directionally coupled, resulting in enhanced translational response.

(4) Regarding rotational motion, the results show that roll and pitch responses exhibit distinct directional dependence. At 0° wave incidence, pitch motion dominates while roll remains relatively small. Conversely, at 90° incidence, roll becomes more significant and pitch is reduced. Under oblique wave directions, both roll and pitch responses increase due to asymmetric excitation and motion coupling effects. Nevertheless, the rotational amplitudes remain within controlled limits and do not indicate instability or excessive dynamic amplification.

Although the motion dataset consists of two representative tables, the observed trends are physically consistent and directly correlated with the mooring tension results. The reduction of motion amplitude with increasing draft corresponds to the decrease in peak mooring tension, confirming that rigid-body motion is the primary driver of mooring load variations. Similarly, the identification of oblique wave incidence as the most demanding horizontal condition aligns with the governing tension case determined in Section 4.1.3. Therefore, even with limited tabulated data, the results provide coherent and mechanistically supported conclusions regarding the global dynamic behavior of the system.

In summary, the eight-point symmetric mooring configuration effectively constrains surge, sway, roll, and pitch motions under all tested environmental combinations. Draft plays a dominant role in enhancing hydrostatic stability and reducing dynamic response, while oblique wave incidence represents the most critical directional condition for horizontal displacement. The motion analysis, together with the tension results, confirms the overall stability and directional robustness of the Octabuoy platform in shallow-water installation scenarios.

4.3. Redundancy Performance under Single-Line Failure

To evaluate the structural redundancy and extreme safety margin of the mooring system, a single-line failure scenario was investigated under the most unfavorable condition identified in

 doi:10.20944/preprints202605.1032.v1

previous analyses, namely the 9.5 m draft combined with the Case 2 sea state. Since this configuration corresponds to the governing design condition in terms of peak mooring tension, it represents the most critical baseline for assessing post-failure behavior.Two representative wave incidence angles (0° and 22.5°) were selected for the failure simulations, and the No.1 mooring line located on the windward side was assumed to be disconnected. The objective of this analysis is to examine load redistribution characteristics, symmetry evolution, and the possibility of progressive failure.

（1）The results demonstrate that after the removal of one mooring line, the system reaches a new equilibrium state without triggering any secondary line failure. The remaining mooring lines redistribute the environmental loads through the coupled restoring mechanism of the symmetric configuration. No evidence of progressive or cascading failure is observed in all tested scenarios, indicating that the overall structural integrity of the eight-point system remains stable under extreme asymmetric disturbance.

（2）Under the 22.5° incidence condition, which represents the most unfavorable directional loading case, the tension previously carried by the failed No.1 line is primarily transferred to the two adjacent lines (No.2 and No.8). These lines experience noticeable tension increases due to their geometric proximity to the original load direction. In contrast, the mooring lines located on the leeward side exhibit relatively minor variations, and the overall distribution remains approximately symmetric with respect to the new equilibrium orientation of the platform.Although the peak tensions in the adjacent lines increase significantly after failure, all values remain below the specified breaking load and satisfy the required safety factor. This indicates that the system possesses sufficient strength reserve to accommodate sudden loss of a single mooring element even under extreme environmental excitation.

（3）For the 0° incidence condition, a similar load redistribution pattern is observed; however, the symmetry breaking effect is less pronounced compared with the oblique case. The failed line's load is mainly shared by the two symmetric neighbors, while the remaining lines experience limited variation. The tension distribution adjusts to a new quasi-equilibrium configuration without exhibiting instability or abnormal amplification.

From a mechanics perspective, the redundancy of the system originates from its geometric symmetry and multi-directional load-sharing capability. The eight-line configuration provides multiple alternative load paths in the horizontal plane. When one line fails, the restoring forces are automatically rebalanced through vector superposition among the remaining lines. This mechanism prevents excessive stress concentration and ensures that no single line becomes critically overloaded.Importantly, no progressive failure phenomenon is detected during the experiments. The redistribution of loads does not lead to tension exceeding the breaking threshold in neighboring lines, confirming that the system maintains adequate global stiffness and structural robustness even under asymmetric damage conditions.

The single-line failure analysis therefore verifies that the Octabuoy eight-point mooring system exhibits strong redundancy performance. Even under the governing extreme sea state and worst-case draft condition, the platform retains its station-keeping capability, and the remaining mooring lines operate within acceptable safety limits. This demonstrates that the symmetric mooring arrangement not only ensures directional load balance during intact conditions but also provides effective damage tolerance in accidental scenarios.

 doi:10.20944/preprints202605.1032.v1

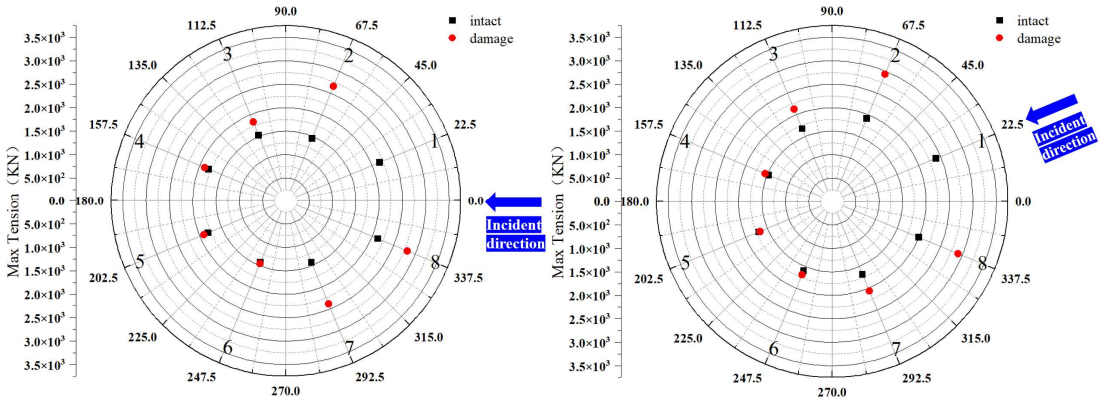

(a) 0° Incidence Angle (b) 22.5° Incidence Angle

Figure 13. Mooring Cable Tension Analysis.

5. Conclusions

Based on the wave basin model tests, the mooring tension characteristics and motion responses of the Octabuoy-type eight-pontoon semi-submersible wind installation platform were systematically investigated under various environmental loading conditions, different wave incidence angles, and multiple draft configurations. Furthermore, the redundancy performance and safety margins under single-line failure conditions were evaluated. Through comprehensive comparative analysis of the experimental results, the following main conclusions are drawn:

(1) The proposed eight-point all-steel symmetric mooring system enables effective load distribution under multidirectional environmental loading. In the intact configuration, the system demonstrates strong horizontal restoring capability and high overall stiffness. Under the most unfavorable environmental combination, the minimum safety factor reaches 2.11, exceeding the design requirement of 1.67, indicating sufficient safety margin in extreme sea states. Under single-line failure conditions, the system remains stable, with a minimum safety factor of 1.7. No cascading failure was observed, confirming the structural redundancy and stability advantages provided by the eight-point symmetric layout.

(2) The mooring stiffness and ultimate loading tests demonstrate that the system maintains favorable restoring performance even under horizontal loads approaching the breaking capacity. When subjected to near-limit horizontal loading under fully taut conditions, the platform returned close to its original equilibrium position after unloading, with a residual displacement of approximately 0.15 m at prototype scale. Under irregular wave, wind, and current coupling effects, the platform motion primarily exhibits periodic oscillations without sustained drift or instability amplification. This indicates that the eight-point mooring system provides reliable station-keeping capability. Such stable restoring characteristics are of significant engineering importance for ensuring operational continuity and safety during wind turbine installation.

(3) The mooring tension and motion responses show clear sensitivity to environmental parameters. Results indicate that increasing draft generally reduces both peak mooring tension and motion amplitudes, suggesting that larger draft enhances system stability and safety margin. Within the scope of this study, the 9.5 m draft represents the governing design condition. Additionally, relatively higher tensions and motion responses occur under 22.5° and 67.5° incident angles, primarily due to load projection effects associated with the symmetric eight-point configuration. These findings provide a clear basis for future engineering design and load case verification.

(4) The single-line failure tests confirm that the eight-point symmetric mooring structure possesses strong load redistribution capability. After the failure of one mooring line, environmental loads are automatically transferred to adjacent lines without triggering global instability or cascading collapse. The tensions in the remaining lines remain within safe limits, and the platform maintains

 doi:10.20944/preprints202605.1032.v1

its fundamental station-keeping function. This demonstrates that the mooring system satisfies safety and reliability requirements under extreme conditions.

In summary, this study experimentally validates the safety, stability, and redundancy performance of the eight-point symmetric all-steel mooring system for the Octabuoy platform through systematic wave basin testing. The governing design conditions were identified, and the influence of draft and wave incidence angle on mooring performance was clarified. The results provide experimental evidence and design reference for the engineering application of such eight-pontoon wind installation platforms in shallow-water regions..

Author Contributions: Conceptualization, X.X. and Y.Y.; methodology, X.X.; software, X.X.; validation, Haitao Xu; formal analysis, X.X.; investigation, X.X.; resources, Hong Zhou.; data curation, X.X.; writing—original draft preparation, Haitao Xu.; writing—review and editing, Hong Zhou.; visualization, X.X.; supervision, X.X.; project administration, Hong Zhou.; funding acquisition, Y.Y. All authors have read and agreed to the published version of the manuscript.

Funding: This research received no external funding.

Informed Consent Statement: Written informed consent has been obtained from the patient(s) to publish this paper.

Conflicts of Interest: The funders had no role in the design of the study; in the collection, analyses, or interpretation of data; in the writing of the manuscript; or in the decision to publish the results.

References

1. Arias, R.R.; Ruiz, A.R.; de Lena Alonso, V.G. Mooring and anchoring. In: Floating Offshore Wind Farms; 2016; pp. 89-119.
2. Chandrasekaran, S. Offshore Semi-submersible Platform Engineering; CRC Press: Boca Raton, FL, USA, 2020.
3. Chandrasekaran, S.; Uddin, S.A.; Wahab, M. Dynamic analysis of semisubmersible under the postulated failure of re-straining system with buoy. International Journal of Steel Structures 2021, 21, 118-131.
4. Ye, X.J.; Zheng, P.Z.; Qiao, D.S.; et al. Multi-objective optimization design of a mooring system based on the surrogate model. Journal of Marine Science and Engineering 2024, 12, 1853.
5. Hennø, E.; Schøyen, H. A lean approach to comparing the mooring systems of Suezmax tankers. Journal of Marine Science and Technology 2024, 29, 1-19.
6. Tang, Y.C.; Chen, X.; Huang, G.Z.; et al. Dynamic analysis of multi-module floating photovoltaic platforms with composite mooring system by considering tidal variation and platform configuration. Ocean Engineering 2024, 312, 119243.
7. Wang, H.W.; Wen, J.; Ma, G.; et al. Coupled dynamics analysis of floating wind turbine mooring system under extreme operating gust. Applied Ocean Research 2025, 154, 104333.
8. Wang, H.W.; Ran, Q.G.; Ma, G.; et al. Optimization design of floating offshore wind turbine mooring system based on DNN and NSGA-III. Ocean Engineering 2025, 316, 119915.
9. Bian, J.H.; Wan, L.; Yang, Y.; et al. Dynamic response analysis of alternative mooring system designs for a 15 MW floating wind turbine with an emphasize on different limit state. Ocean Engineering 2025, 315, 119787.
10. Huang, J.W.; Xu, H.; Chen, L.; et al. Analysis of mooring performance and layout parameters of multi-segment mooring system for a 15 MW floating wind turbine. Frontiers in Energy Research 2024, 12, 1502684.
11. Neisi, A.; Ghassemi, H.; Iranmanesh, M. Dynamic response of three different floating platform (OC4, BSS, GVA) using multi-segment mooring system. Applied Ocean Research 2024, 153, 104301.
12. Chern, F.L.; Sindre, F.; Muk, C.O. Design and analysis of taut mooring systems for a combined floating offshore wind and wave energy system at intermediate water depth. Ocean Engineering 2024, 312, 119174.

 doi:10.20944/preprints202605.1032.v1

13. Nguyen, H.P.; Huang, C.X.; von Herzen, B.; et al. Numerical study on hydroelastic responses of submersible high-density polyethylene circular seaweed platforms held by single-point mooring system and buoys. Journal of Marine Science and Engineering 2024, 12, 1437.
14. Mujeeb-Ahmed, M.P.; Cabrera, J.; Kim, H.J.; et al. Effect of mooring line layout on the loads of ship-shaped offshore installations. Ocean Engineering 2021, 241, 110071.
15. Li, L.; Jiang, Z.; Ong, M.C.; et al. Design optimization of mooring system: an application to a vessel-shaped offshore fish farm. Engineering Structures 2019, 197, 109363.
16. Ma, K.; Shu, H.; Smedley, P.; et al. A historical review on integrity issues of permanent mooring systems. In: Proceedings of the Offshore Technology Conference; OTC: Houston, TX, USA, 2013; OTC-24025-MS.
17. Pham, H.D.; Cartraud, P.; Schoefs, F.; et al. Dynamic modeling of nylon mooring lines for a floating wind turbine. Applied Ocean Research 2019, 87, 1-8.
18. Tang, H.Y.; Yang, R.Y.; Yao, H.C. Experimental and numerical investigations of a mooring line failure of an aquaculture net cage subjected to currents. Ocean Engineering 2021, 238, 1-11.
19. Vazquez-Hernandez, A.O.; Ellwanger, G.B.; Sagrilo, L.V.S. Long-term response analysis of FPSO mooring systems. Applied Ocean Research 2011, 33(4), 375-383.
20. Chen, Z.W.; Jiao, J.L.; Chang, X.; et al. Numerical and experimental study of asymmetrical wave loads and hydroelastic responses of ship in oblique regular waves. Applied Ocean Research 2024, 153, 104254.
21. Han, W.H.; Yu, X.; Wang, J.J.; et al. Extreme wave-induced pressure distribution and wave forces on tandem pile groups: an experimental study. Journal of Marine Science and Engineering 2024, 12(9), 1674.
22. Mao, H.F.; Zeng, J.W.; Wu, G.L.; et al. Characteristics of higher harmonic forces on submerged horizontal cylinders with sharp and round corners. Journal of Marine Science and Engineering 2024, 12, 1636.
23. Mao, H.F.; Yang, Y.T.; Jin, B.L.; et al. Numerical examination of wave forces on partially submerged horizontal circular cylinders near free surface. Ocean Engineering 2024, 313, 119497.
24. Fan, Y.P.; Li, J.X.; Liu, S.X.; et al. A study of wave forces on a vertical truncated cylinder with different submergence depths. Ocean Engineering 2024, 313(P2), 119489.
25. Tang, T.N.; Ding, H.Y.; Dai, S.S.; et al.; Adcock, T.A.A. An experimental study of a quasi-impulsive backwards wave force associated with the secondary load cycle on a vertical cylinder. Journal of Fluid Mechanics 2024, 994, A9.
26. Tian, X.J.; Liu, Y.X.; Liu, G.J.; et al. Experimental study on influencing factors of hydrodynamic coefficient for jack-up platform. Ocean Engineering 2019, 193, 106588.
27. Liu, L.; Yang, J.M.; Tian, X.L.; et al. Experimental investigation on the hydrodynamic performance of a quay moored jackup. Ships and Offshore Structures 2017, 12, 679-689.
28. Dymarski, C.; Dymarski, P. Developing methodology for model tests of floating platforms in low-depth towing tank. Archives of Civil and Mechanical Engineering 2016, 16, 159-167.
29. Liang, M.; Wang, X.; Xu, S.; et al. A shallow water mooring system design methodology combining NSGA-II with the vessel-mooring coupled model. Ocean Engineering 2019, 190, 106417.
30. Li, L.; Jiang, Z.; Ong, M.C.; et al. Design optimization of mooring system: an application to a vessel-shaped offshore fish farm. Engineering Structures 2019, 197, 109363.
31. Wang, H.M.; Lu, K.; Liang, S.G. Experimental study on hydrodynamic characteristics of anchored offshore test platform under wind wave current coupling. Proceedings of SPIE 2023, 12793, 127931S-1-127931S-12.
32. Wang, H.W.; Ran, Q.G.; Ma, G.; et al. Optimization design of floating offshore wind turbine mooring system based on DNN and NSGA-III. Ocean Engineering 2025, 316, 119915.
33. Tang, H.J.; Yeh, P.H.; Huang, C.C.; et al. Numerical study of the mooring system failure of aquaculture net cages under irregular waves and current. Ocean Engineering 2020, 216, 1-12.
34. Ibarra, M.A.C.; Simao, M.L.; Videiro, P.M.; et al. Long-term fatigue analysis of mooring lines considering wind-sea and swell waves using the univariate dimension-reduction method. Applied Ocean Research 2022, 118, 1-16.
35. Bae, Y.H.; Kim, M.H.; Kim, H.C. Performance changes of a floating offshore wind turbine with broken mooring line. Renewable Energy 2017, 101, 364-375.
36. Li, Y.; Zhu, Q.; Liu, L.Q.; et al. Transient response of a SPAR-type floating offshore wind turbine with fractured mooring lines. Renewable Energy 2018, 122, 576-588.

 doi:10.20944/preprints202605.1032.v1

37. Le, C.H.; Li, Y.; Ding, H.Y. Study on the coupled dynamic responses of a submerged floating wind turbine under different mooring conditions. Energies 2019, 12(3), 1-21.
38. Chuang, Z.J.; Chang, X.; Li, C.Z.; et al. Performance change of a semi-submersible production platform system with broken mooring line or riser. Engineering Failure Analysis 2020, 118, 1-18.
39. Arief, I.S.; Utama, I.K.A.P.; Hantoro, R.; et al. Mooring experimental study of motion response for pendulum wave energy converters. IOP Conference Series: Materials Science and Engineering 2019, 462(1).
40. Chern, F.L.; Sindre, F.; Muk, C.O. Design and analysis of taut mooring systems for a combined floating offshore wind and wave energy system at intermediate water depth. Ocean Engineering 2024, 312, 119174.
41. Li, J.W.; Zuo, H.L.; Zuo, J.J.; et al. Study on the mooring systems attaching clump weights and heavy chains for improving the typhoon resistance of floating offshore wind turbines. Ocean Engineering 2024, 311, 118734.
42. Yu, J.; Cheng, X.M.; Xie, C.M.; et al. Hydrodynamic analysis of three-module semi-submersible platform and its mooring design. Ocean Engineering 2024, 310, 118576.
43. Chen, M.S.; Jiang, J.L.; Zhang, W.; et al. Study on mooring design of 15 MW floating wind turbines in South China Sea. Journal of Marine Science and Engineering 2023, 12(1).